

Accepted Manuscript

Accepted Manuscript (Uncorrected Proof)

Title: A Full Wave Solution of Deep Sources in the Lossy Human Head to Accurate EEG and MEG

Authors: Sattar Samadi¹, Bijan Zakeri^{1,*}, Reza Khanbabaie²

1. Department of Electrical Engineering, Babol Noshirvani University of Technology, Babol, Iran.
2. Department of Physics, University of British Columbia, Canada.

***Corresponding Author:** Email: zakeri@nit.ac.ir

To appear in: **Basic and Clinical Neuroscience**

Received date: 2021/10/28

Revised date: 2022/02/26

Accepted date: 2022/04/12

This is a “Just Accepted” manuscript, which has been examined by the peer-review process and has been accepted for publication. A “Just Accepted” manuscript is published online shortly after its acceptance, which is prior to technical editing and formatting and author proofing. *Basic and Clinical Neuroscience* provides “Just Accepted” as an optional and free service which allows authors to make their results available to the research community as soon as possible after acceptance. After a manuscript has been technically edited and formatted, it will be removed from the “Just Accepted” Web site and published as a published article. Please note that technical editing may introduce minor changes to the manuscript text and/or graphics which may affect the content, and all legal disclaimers that apply to the journal pertain.

Please cite this article as:

Samadi, S., Zakeri, B., & Khanbabaie, R. (In Press). A Full Wave Solution of Deep Sources in the Lossy Human Head to Accurate EEG and MEG. *Basic and Clinical Neuroscience*. Just Accepted publication Aug. 15, 2022. Doi: <http://dx.doi.org/10.32598/bcn.2022.3821.1>
DOI: <http://dx.doi.org/10.32598/bcn.2022.3821.1>

Abstract

In this paper, by using the electromagnetic modeling of the neuron activity and human head, its electric and magnetic fields (brain waves) have been derived in the full-wave approach (*i.e. without any approximation*). Traditionally -and of course currently- the brain waves are only derived by using the quasi-static approximation (QSA) of Maxwell's equations in electromagnetic theory and therefore, source localization in brain imaging will have some errors. So far, the error rate of the QSA on the *output* results of electric and magnetic fields has not been investigated. This issue becomes more noticeable due to increased sensitivity of recent modern electroencephalography (EEG) and magnetoencephalography (MEG) devices. In this work, first, issues that QSA encountered in this problem are introduced and the necessity of full wave solution is revealed and then, for the first time, the full-wave solution of the problem in closed form format is presented. This solution is done in two scenarios: 1- the source (active neurons) in the center of a sphere and 2- the source in the out of center but deeply inside the sphere. First scenario is simpler but the second scenario is much more complicated and has been solved by using partial-wave series expression (PWSE). One of the important achievements of this modelling is improving the interpretation of EEG and MEG measurement resulting in more accurate source localization.

Keywords: Brain waves, Quasi-static approximation, Full-wave analysis, Brain imaging, Human head modelling

Accepted Manuscript (Uncorrected Proof)

I-Introduction

Currents in the brain flow inside neurons and across their boundaries into the extracellular medium producing the electric and magnetic fields. These fields, that contain suitable information of the brain activity, can be measured by electroencephalography (EEG), magnetoencephalography (MEG) as well as by direct neural imaging (DNI). One of important issues in recognizing of brain disorders and cognitive functions is detection of the location and distribution of active neurons in the brain from measured electric and magnetic fields. This is known as the inverse problem. To handle inverse problem, it is necessary to provide a mathematical model that links neuronal sources to measured signals. This is known as forward problem that calculates the electric and magnetic field produced by a predefined neuronal current in a special location [1-2].

In analytical studies, a number of mathematical-electromagnetic models have been used to explain the forward problem in the past few decades [3-6]. A key part of all these models is a volume conductor model that characterizes the effect of head conductivity and permittivity profile on neutrally driven electric currents. The analytic solution is given for different conductivity profile: a single homogenous sphere [7], multilayer non-isotropic sphere [8-9] and even though for slightly more realistic spheroidal [10-11] and ellipsoidal [12] geometries.

Due to low-frequency nature of brain activity, all of these models have been derived only by quasi-static approximation (QSA) of Maxwell-equations [13]. QSA enables Maxwell's equations to be simplified by ignoring capacitive, inductive and wave propagation effects [14]. While the extracellular potential is thought to be exclusively generated by the transmembrane currents, the recent studies suggest that the extracellular diffusive, advective and displacement currents may also contribute considerably toward extracellular potential recordings [15-17]. However, QSA implicitly assumes that the tissue conductivity is independent of the frequency in the physiological ranges, and that the diffusion, advection and displacement currents are negligible in comparison to conductive return current [15].

For overcome QSA's issues, we have derived a full-wave analytical expression for the electric and magnetic field of a current dipole positioned into a homogenous conductor sphere. The full-wave analysis results the enrichment of information obtained from EEG/MEG measurements. To start the full-wave solution, we assume that the source is a small current dipole placed into scatterer (sphere). Due to angular dependence of the field components in the boundary, this is explored by utilizing the partial-wave series expression (PWSE) technique. The PWSE is a technique for solving scattering problems by decomposing constituent angular components of fields to applying boundary conditions [18-19].

This paper is organized as follows. In Section II, the background knowledge about the generation of EM fields by the neurons is presented. Then the traditional role of QSA in the solution of EM fields as well as related references is introduced. Then, some landmark notes and objections about applicant of QSA in EEG/MEG forward problem. In section III, the theoretical equations for the full-wave EEG/MEG forward problem is developed. This is done in two scenarios: the centered source and off-center source. For this purpose, the scattering problem for a current dipole inside a sphere is solved using the PWSE technique. Section VI represents the numerical computations and simulation results to illustrate the theory. Section V deals with the convergence of the addition theorem as one of the main challenge of this work. Finally, in the section VI, the conclusions are presented.

II-Problem Overview

A- Proposed Scheme

In this section we introduce the electromagnetic model of an active neuron inside the brain. When a neuron is activated, a primary current (\mathbf{J}^P) flows into it. Because the neurons are located in an electrically conducting medium, the extracellular current that called the return current (\mathbf{J}^R) follows a path that depends upon the conductivity profile of the extracellular medium. The return current is

ohmic current that is taken to be the product of the local conductivity σ and the electric field \mathbf{E} ($\mathbf{J}^R = \sigma \mathbf{E}$). So, the total current is $\mathbf{J} = \mathbf{J}^P + \sigma \mathbf{E}$. Both the primary and return currents contribute to the formation of the electric and magnetic field. Figure 1 conceptually shows an active neuron with primary and return currents with induced electric and magnetic fields near it.

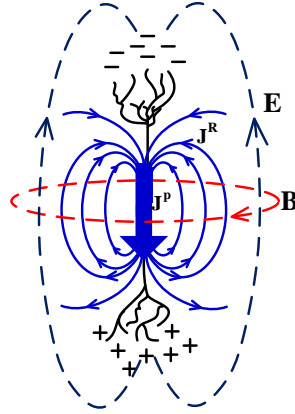


Fig. 1. A conceptual representation of an active neuron with volume current distribution and electric and magnetic fields

Since the length of a neuron is negligible compared with the head size, it is assumed that all the primary current concentrated at a single position \mathbf{r}' has a moment of \mathbf{p} . Thus the primary current is described by equivalent current dipole (ECD) and mathematically is written as $\mathbf{J}^P(\mathbf{r}) = \mathbf{p} \delta^3(\mathbf{r} - \mathbf{r}')$ where δ is the Dirac delta function. Among different ways to modelling of neurons as current source, ECD is widely used in clinical applications [20].

In the forward problem, the electric and magnetic fields have been determined from the neuronal current distribution. This is done by the classical electromagnetic theory that is described in Maxwell's equations as follows:

$$\nabla \times \mathbf{E} = -\frac{\partial \mathbf{B}}{\partial t}, \quad \nabla \times \mathbf{B} = \mu \mathbf{J} + \mu \frac{\partial \mathbf{D}}{\partial t}, \quad \nabla \cdot \mathbf{D} = 0, \quad \nabla \cdot \mathbf{B} = 0 \quad (1)$$

Where \mathbf{E} , \mathbf{B} , \mathbf{J} and $\frac{\partial \mathbf{D}}{\partial t}$ are the electric field, magnetic field, current source density and displacement current density respectively. Traditionally, because of low frequency of neuronal activities, in all corresponding articles and books, the formulations is done based on the QSA, i.e. ignoring of time varying terms (i.e. $\frac{\partial \mathbf{B}}{\partial t}$ and $\frac{\partial \mathbf{D}}{\partial t}$) in the Maxwell's equations. The argument is that because the two inequality $2\pi f \varepsilon / \sigma \ll 1$ and $\mu_0 \sigma 2\pi f R^2 \ll 1$ are hold, so we can use QSA. In those two inequality, f is frequency of neuronal activity, μ_0 , ε and σ are the constitutive parameters of the brain tissue as well as R is the radius of the human head [21-22].

Based on QSA, the analytic solution of forward problem for special geometries of head model has been introduced [23-24]. One of the most important geometry is spherical in which the electrical conductivity is assumed to be depended only on the distance from the origin [25]. This shape approximates the shape of the human head and can serve as a basis for understanding the measurements of the brain's electric and magnetic fields [4]. Basically, the starting point to derive these field equations is attempting to solve the problem for a simple homogeneous sphere [4]. Derivation of analytical solutions for simplified geometries (such as sphere) has important roles in EEG/MEG tests interpretation, including: leading to useful rules-of-thumb, calibration of EEG/MEG equipment, verifying numerical methods for realistic model geometries and etc.

B- QSA Challenges

As mentioned earlier, due to low frequency nature of neuron activities, the time varying terms in Maxwell's equations has been ignored and QSA is established. But there is some objections and significant challenges about this establishment as follows:

Issue 1. In physical problems, when a data is the sum of two or more components so that one of them is much smaller than the other, from an engineering point of view the smallest component is usually ignored (such as ignoring high-order sentences in the Taylor's Expansion). In all literatures, from 1967 [26] right now, by arguing that the time variant terms in Maxwell's equations (i.e. $\frac{\partial B}{\partial t}$ and $\frac{\partial D}{\partial t}$ terms in equation (1)) is negligible, the form of Maxwell's equations is reduced to the quasi-static form. Although this simplifies problem solving but may lose valuable information. However this ignorations should be *quantitatively* investigated to evaluate the electric and magnetic fields. There is not any report that uses the perfect form of Maxwell's equations (full-wave form) to measure the quasi-static errors. Recent advances in neuronal current imaging using more sensitive EEG/MEG devices, as well as better shielding techniques, have made it possible to measure the smallest changes in electric and magnetic fields. Recently there is an EEG with an accuracy level of $2.7nv/\sqrt{Hz}$ [27-28] and a MEG with an accuracy level of $0.01fT \sqrt{cm^3/Hz}$ [29-30]. So, it seems even if the difference between the quasi-static and full-wave results is too low, this difference is detectable with today's modern devices.

Issue 2. It is already mentioned that one of the conditions that establish a quasi-static approximation is $2\pi f\epsilon/\sigma \ll 1$ [22]. For inside the head, this condition is correct unlike the outside. Because in the outside of head, $\sigma = 0$ and then $2\pi f\epsilon/\sigma \rightarrow \infty$. Thus, for the outside of the head, time varying terms are considerable.

Issue 3. In [15] it is emphasized that, the displacement current ($\partial D/\partial t$) in Ampere–Maxwell's law is responsible for the capacitive charging of neural membranes and cannot be neglected. Furthermore, in [31] it is stated that: “since the goal of the inverse source problem is the monitor of dynamic neuronal events (an action potential has a rise time on the order of 0.5ms [32]), it may be that the displacement current is not negligible. This has already been pointed out in studies of source problems related to monitoring neurons in the arm [33]”.

Issue 4. In all argumentations presented to ignoring of time-varying terms in Maxwell equations, it is assumed that the brain media is the linear, isotropic and homogeneous. While the human brain does not really have these properties [34].

These uncertainties encourage us –for first time– to solve the forward problem by the full wave method instead of QSA. As well-known in electromagnetic theory, the full-wave solution of an electromagnetic problem gives the *full* solution (including time varying terms) not an approximation and thus above issues has been automatically are resolved. In the next section we establish the full-wave analysis formulation of the problem for two scenarios: one for a centered source and another for an off-center source.

III- The Full Wave Solution of the Forward Problem

In this section we want to introduce the relationships that are very convenient for solving scattering of waves emanating from a finite source placed in a spherical object (scatterer). Let us consider a homogenous conductor sphere of radius R and electromagnetic parameters of ϵ_r and σ . Assume that the medium outside the sphere is free space (wave number β_0) and inside is a lossy dielectric (wave number $\hat{\beta}_d$) represented by a relative complex permittivity $\hat{\epsilon}_d$ ($\hat{\epsilon}_d = \epsilon_0\epsilon_r - j\frac{\sigma}{\omega}$). Depend on the source location inside the sphere (either center or out of center), the formulation path can be different. For this, we represent our formulations into two scenarios: one for centered source and another for

off-centered source. These scenarios is shown in the following figure.

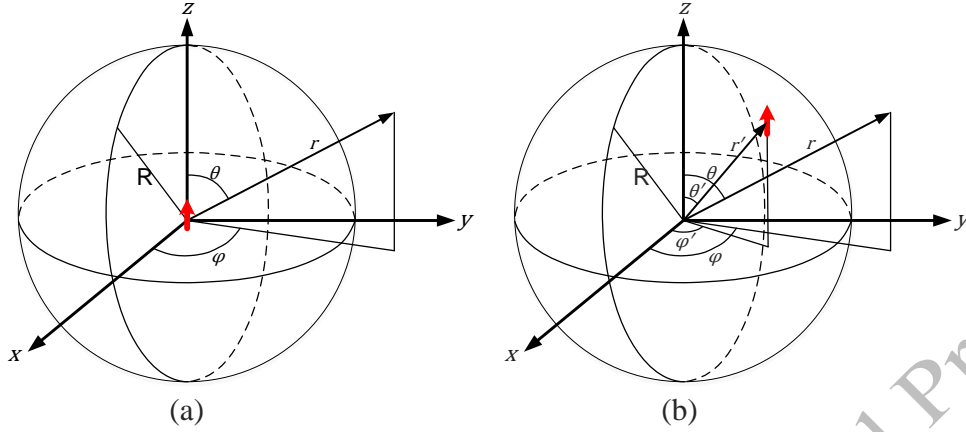


Fig. 2. The current dipole in the structure under study (a) the current dipole in the center. (b) The current dipole in the arbitrary off-center location.

A- Source Origin

We start the solution of the problem in simplest situation, i. e., a source in the center of the desired sphere. Figure 2-a shows the geometry of the problem. As can be seen, a current dipole, i.e. a very thin linear electric current element of very short length ($l \ll \lambda$) and a constant current I , as a neuron source is positioned at the center of the sphere. The problem is finding the EM field in both inside and outside of the conductor sphere. To this, we use the magnetic vector potential \mathbf{A} defined in electromagnetic terminology. The dipole's incident field can be represented by \mathbf{A} as [35]:

$$\mathbf{A} = A_r^i \mathbf{a}_r = a \hat{H}_1^{(2)}(\beta_d r) P_1(\cos\theta) \mathbf{a}_r, \quad a = \frac{j\mu_0 \beta_d l I}{4\pi} \quad (2)$$

where $\beta_d = \omega \sqrt{\mu \epsilon_r}$ is the wave number, $\hat{H}_1^{(2)}$ is Schelkunoff spherical Hankel function of the second kind, P_1 is the Legendre function of the first kind and lI is the current dipole moment. The index i in A_r^i is referred to incident field from source to the bounded media. Upon the interaction of the electromagnetic wave with the sphere in its boundary, the scattered beam is composed of two part, namely inside scattered wave (A_r^{s-}) and outside scattered wave (A_r^{s+}). Because the field must be finite everywhere in the sphere, including $r=0$, and has standing form, the inside scattered wave written as:

$$A_r^{s-} = b \hat{J}_1(\beta_d r) P_1(\cos\theta) \quad (3)$$

In the outside of the sphere the field must has travelling form as:

$$A_r^{s+} = c \hat{H}_1^{(2)}(\beta_0 r) P_1(\cos\theta) \quad (4)$$

In these equations, b and c is the sphere scattering coefficients to be determined by applying appropriate boundary conditions. The total vector potential inside the sphere is $A_r^{t-} = A_r^i + A_r^{s-}$ and outside is $A_r^{t+} = A_r^{s+}$. Thus, the electric and magnetic fields obtain from the following equations by eliminating the zero components [35].

$$E_r = \frac{1}{j\omega\mu\epsilon} \left(\frac{\partial^2}{\partial r^2} + \beta^2 \right) \psi, \quad E_\theta = \frac{1}{j\omega\mu\epsilon r} \frac{\partial^2 \psi}{\partial r \partial \theta}, \quad H_\phi = -\frac{1}{\mu r} \frac{\partial \psi}{\partial \theta} \quad (5)$$

In which $\psi = A_r^{t-}$ for $r \leq R$ and $\psi = A_r^{t+}$ for $r > R$. The tangential components of the fields inside and outside the sphere are derived as:

$$E_{\theta}^{t-} = \frac{1}{j\omega\mu\epsilon_d r} \left[-a\beta_d \hat{H}_0^{(2)}(\beta_d r) \sin\theta + \frac{a}{r} \hat{H}_1^{(2)}(\beta_d r) \sin\theta - b\beta_d \hat{J}_0(\beta_d r) \sin\theta + \frac{b}{r} \hat{J}_1(\beta_d r) \sin\theta \right] \quad (6)$$

$$E_{\theta}^{t+} = \frac{1}{j\omega\mu\epsilon_0 r} \left[-c\beta_0 \hat{H}_0^{(2)}(\beta_0 r) \sin\theta + \frac{c}{r} \hat{H}_1^{(2)}(\beta_0 r) \sin\theta \right] \quad (7)$$

$$H_{\phi}^{t-} = -\frac{1}{\mu r} \left[-a\hat{H}_1^{(2)}(\beta_d r) \sin\theta - b\hat{J}_1(\beta_d r) \sin\theta \right] \quad (8)$$

$$H_{\phi}^{t+} = -\frac{1}{\mu r} \left[-c\hat{H}_1^{(2)}(\beta_0 r) \sin\theta \right] \quad (9)$$

By applying the boundary conditions on $r = R$:

$$E_{\theta}^{t+}(r = R) = E_{\theta}^{t-}(r = R) \quad , \quad H_{\phi}^{t+}(r = R) = H_{\phi}^{t-}(r = R) \quad (10)$$

The coefficients b and c are determined as:

$$b = \frac{M_b + N_b}{O_b + P_b} \quad , \quad c = \frac{M_c + N_c}{O_c + P_c} \quad (11)$$

where:

$$M_b = \epsilon_0 \beta_d \hat{H}_0^{(2)}(\beta_d R) \hat{H}_1^{(2)}(\beta_0 R) - \frac{\epsilon_0}{R} \hat{H}_1^{(2)}(\beta_d R) \hat{H}_1^{(2)}(\beta_0 R) \quad (12)$$

$$N_b = -\epsilon_d \beta_0 \hat{H}_0^{(2)}(\beta_0 R) \hat{H}_1^{(2)}(\beta_d R) + \frac{\epsilon_0}{R} \hat{H}_1^{(2)}(\beta_d R) \hat{H}_1^{(2)}(\beta_0 R) \quad (13)$$

$$O_b = \epsilon_d \beta_0 \hat{H}_0^{(2)}(\beta_0 R) \hat{J}_1(\beta_d R) - \frac{\epsilon_d}{R} \hat{H}_1^{(2)}(\beta_0 R) \hat{J}_1(\beta_d R) \quad (14)$$

$$P_b = -\epsilon_0 \beta_d \hat{J}_0(\beta_d R) \hat{H}_1^{(2)}(\beta_0 R) + \frac{\epsilon_0}{R} \hat{J}_1(\beta_d R) \hat{H}_1^{(2)}(\beta_0 R) \quad (15)$$

$$M_c = \epsilon_0 \beta_d \hat{H}_0^{(2)}(\beta_d R) \hat{J}_1(\beta_d R) - \frac{\epsilon_0}{R} \hat{H}_1^{(2)}(\beta_d R) \hat{J}_1(\beta_d R) \quad (16)$$

$$N_c = -\epsilon_0 \beta_d \hat{J}_0(\beta_d R) \hat{H}_1^{(2)}(\beta_d R) + \frac{\epsilon_0}{R} \hat{J}_1(\beta_d R) \hat{H}_1^{(2)}(\beta_d R) \quad (17)$$

$$O_c = \epsilon_d \beta_0 \hat{H}_0^{(2)}(\beta_0 R) \hat{J}_1(\beta_d R) - \frac{\epsilon_d}{R} \hat{H}_1^{(2)}(\beta_0 R) \hat{J}_1(\beta_d R) \quad (18)$$

$$P_c = -\epsilon_0 \beta_d \hat{J}_0(\beta_d R) \hat{H}_1^{(2)}(\beta_0 R) + \frac{\epsilon_0}{R} \hat{J}_1(\beta_d R) \hat{H}_1^{(2)}(\beta_0 R) \quad (19)$$

B- Source Off-Origin

Now we assume that the source is positioned at out of the center in point $\mathbf{r}' = (r', \theta', \varphi')$ and oriented along z-axis. Figure 2-b shows the structure. Note that assumption of the removable z-directed dipole in the problem doesn't detract the generality of the problem because the sphere is perfectly symmetrical. The magnetic vector potential is [35]:

$$\mathbf{A}^i = \hat{\mathbf{a}}_z A_z^i = \hat{\mathbf{a}}_z \frac{\beta_d I l}{4\pi j} h_0^{(2)}(\beta_d |\mathbf{r} - \mathbf{r}'|) \quad (20)$$

where $h_0^{(2)}$ is spherical Hankel function of the second kind. When dealing with spherical wave scattering of waves generated by current dipole radiator located away from the origin at \mathbf{r}' , it is convenient to express its radiation in terms of spherical wave function originating at the origin of the coordinate system. This can be accomplished using the ‘‘addition theorem’’ of spherical wave functions, which states that equation (20) can be expressed as [35]:

$$A_z^i = \begin{cases} \sum_{n=0}^{\infty} \sum_{m=0}^n \varepsilon_m O_{nm} a_n h_n^{(2)}(\beta_a r') j_n(\beta_a r) P_n^m(\cos \theta) P_n^m(\cos \theta') \cos(m(\varphi - \varphi')), & r < r' \\ \sum_{n=0}^{\infty} \sum_{m=0}^n \varepsilon_m O_{nm} a_n h_n^{(2)}(\beta_a r) j_n(\beta_a r') P_n^m(\cos \theta) P_n^m(\cos \theta') \cos(m(\varphi - \varphi')), & r > r' \end{cases} \quad (21)$$

where

$$\varepsilon_m = \begin{cases} 1, & m = 0 \\ 2, & m \neq 0 \end{cases}, \quad O_{nm} = \frac{(n-m)!}{(n+m)!}, \quad a_n = (2n+1) \frac{\beta_a l l}{4\pi j}$$

where $P_n^m(\cdot)$ is the associated Legendre function. The reason of choosing z-directed representation of \mathbf{A} instead of radially directed is that it is not found the addition theorem for the radially directed representation for it. Bessel functions $j_n(\beta r)$ were selected to represent the fields for $r < r'$ because the field must be finite everywhere, including $r = 0$, and Hankel functions were chosen for $r > r'$ to represent the travelling nature of the wave. The expression for the inside scattered wave (\mathbf{A}^{s-}) will be of similar forms as first expression of (21) and for the outside scattered wave (\mathbf{A}^{s+}) will be of similar forms as second expression of (21), and written as:

$$\mathbf{A}^{s-} = \hat{\mathbf{a}}_z A_z^{s-} = \hat{\mathbf{a}}_z \sum_{n=0}^{\infty} \sum_{m=0}^n \varepsilon_m O_{nm} b_n h_n^{(2)}(\beta_a r') j_n(\beta_a r) P_n^m(\cos \theta) P_n^m(\cos \theta') \cos(m(\varphi - \varphi')) \quad (22)$$

$$\mathbf{A}^{s+} = \hat{\mathbf{a}}_z A_z^{s+} = \hat{\mathbf{a}}_z \sum_{n=0}^{\infty} \sum_{m=0}^n \varepsilon_m O_{nm} c_n h_n^{(2)}(\beta_0 r) j_n(\beta_0 r') P_n^m(\cos \theta) P_n^m(\cos \theta') \cos(m(\varphi - \varphi')) \quad (23)$$

where b_n and c_n are the sphere scattering coefficients to be determined by applying appropriate boundary conditions. The superscript minus (-) is used to identify the vector potentials and associated fields on and within the sphere ($r \leq R$), while the plus (+) is used to identify those on and outside the sphere ($r \geq R$).

The appropriate boundary conditions must be applied on the surface of the sphere; continuity of the tangential electric and magnetic fields. It must be derive the total electric and magnetic field in both inside and outside of the sphere. Thus, the total vector potential inside the sphere (\mathbf{A}^{t-}) is composed of the incident plus inside scattered vector potentials ($\mathbf{A}^i + \mathbf{A}^{s-}$) and outside the sphere (\mathbf{A}^{t+}) is only outside scattered vector potential (\mathbf{A}^{s+}). All the components of the total EM fields, incident plus scattered, can be found from vector potential using the following equations:

$$E_r = -j\omega\mu\psi \cos \theta + \frac{1}{j\omega\varepsilon} \frac{\partial}{\partial r} \left[\frac{\cos \theta}{r^2} \frac{\partial}{\partial r} (r^2\psi) - \frac{1}{r \sin \theta} \frac{\partial}{\partial \theta} (\psi \sin^2 \theta) \right] \quad (24)$$

$$E_\theta = j\omega\mu\psi \sin \theta + \frac{1}{j\omega\varepsilon r} \frac{\partial}{\partial \theta} \left[\frac{\cos \theta}{r^2} \frac{\partial}{\partial r} (r^2\psi) - \frac{1}{r \sin \theta} \frac{\partial}{\partial \theta} (\psi \sin^2 \theta) \right] \quad (25)$$

$$E_\varphi = \frac{1}{j\omega\varepsilon r \sin \theta} \frac{\partial}{\partial \varphi} \left[\frac{\cos \theta}{r^2} \frac{\partial}{\partial r} (r^2\psi) - \frac{1}{r \sin \theta} \frac{\partial}{\partial \theta} (\psi \sin^2 \theta) \right] \quad (26)$$

$$B_r = \frac{\mu}{r} \frac{\partial \psi}{\partial \varphi}, \quad B_\theta = \mu \frac{\cot \theta}{r} \frac{\partial \psi}{\partial \varphi}, \quad B_\varphi = \frac{-\mu}{r} \left[\sin \theta \frac{\partial}{\partial r} (r\psi) + \frac{\partial}{\partial \theta} (\psi \cos \theta) \right] \quad (27)$$

In recent equations, if we want electromagnetic fields for inside the sphere let $\psi = A_z^{t-}$ and for outside the sphere let $\psi = A_z^{t+}$. The scattering coefficients b_n and c_n for the sphere can be now be determined after applying the boundary condition to the total tangent electric field. After simplifying and arrangement, this procedure leads to two system of linear equations, one for E_θ and other for E_φ :

$$\sum_{n=0}^{\infty} \sum_{m=0}^n a_n \Gamma_{nm}(\theta, \varphi) + b_n \Lambda_{nm}(\theta, \varphi) - c_n \Pi_{nm}(\theta, \varphi) = 0 \quad \text{for } E_\theta \quad (28)$$

$$\sum_{n=0}^{\infty} \sum_{m=0}^n a_n \Psi_{nm}(\theta, \varphi) + b_n \Phi_{nm}(\theta, \varphi) - c_n \Theta_{nm}(\theta, \varphi) = 0 \quad \text{for } E_\varphi \quad (29)$$

where the functions $\Gamma_{nm}(\theta, \varphi)$, $\Lambda_{nm}(\theta, \varphi)$ and $\Pi_{nm}(\theta, \varphi)$ in equation (28) are expressed, respectively, as:

$$\begin{aligned} \begin{pmatrix} \Gamma_{nm}(\theta, \varphi) \\ \Lambda_{nm}(\theta, \varphi) \\ \Pi_{nm}(\theta, \varphi) \end{pmatrix} &= \cos(m(\varphi - \varphi')) \cdot \begin{pmatrix} A_{nm} \\ B_{nm} \\ F_{nm} \end{pmatrix} \sin \theta P_n^{m''}(\cos \theta) + \begin{pmatrix} A_{nm} + C_{nm} \\ B_{nm} + D_{nm} \\ F_{nm} + G_{nm} \end{pmatrix} \cos \theta P_n^{m'}(\cos \theta) + \\ &\quad \begin{pmatrix} A_{nm}(\dot{\beta}_d R)^2 - C_{nm} \\ B_{nm}(\dot{\beta}_d R)^2 - D_{nm} \\ F_{nm}(\beta_0 R)^2 - G_{nm} \end{pmatrix} \sin \theta P_n^m(\cos \theta) \end{pmatrix} \quad (30)$$

and $\Psi_{nm}(\theta, \varphi)$, $\Phi_{nm}(\theta, \varphi)$ and $\Theta_{nm}(\theta, \varphi)$ in equation (29) are expressed, respectively, as:

$$\begin{pmatrix} \Psi_{nm}(\theta, \varphi) \\ \Phi_{nm}(\theta, \varphi) \\ \Theta_{nm}(\theta, \varphi) \end{pmatrix} = \sin(m(\varphi - \varphi')) \cdot \begin{pmatrix} mA_{nm} \\ mB_{nm} \\ mF_{nm} \end{pmatrix} P_n^{m'}(\cos \theta) + \begin{pmatrix} mC_{nm} \\ mD_{nm} \\ mG_{nm} \end{pmatrix} \frac{1}{\tan \theta} P_n^m(\cos \theta) \quad (31)$$

In equations (30) and (31) the coefficients A_{nm} , B_{nm} , C_{nm} , D_{nm} , F_{nm} and G_{nm} depend only on the structure of the problem (e.g. source position, source moment, frequency, sphere radius, sphere material) as:

$$A_{nm} = \frac{j}{\omega \dot{\epsilon}_d R^2} \epsilon_m O_{nm} h_n^{(2)}(\dot{\beta}_d R) j_n(\dot{\beta}_d r') P_n^m(\cos \theta') \quad (32)$$

$$B_{nm} = \frac{j}{\omega \dot{\epsilon}_d R^2} \epsilon_m O_{nm} h_n^{(2)}(\dot{\beta}_d r') j_n(\dot{\beta}_d R) P_n^m(\cos \theta') \quad (33)$$

$$C_{nm} = \frac{1}{j \omega \dot{\epsilon}_d R} \epsilon_m O_{nm} h_n^{(2)'}(\dot{\beta}_d R) j_n(\dot{\beta}_d r') P_n^m(\cos \theta') \quad (34)$$

$$D_{nm} = \frac{1}{j \omega \dot{\epsilon}_d R} \epsilon_m O_{nm} h_n^{(2)}(\dot{\beta}_d r') j_n'(\dot{\beta}_d R) P_n^m(\cos \theta') \quad (35)$$

$$F_{nm} = \frac{j}{\omega \epsilon_0 R^2} \epsilon_m O_{nm} h_n^{(2)}(\beta_0 R) j_n(\beta_0 r') P_n^m(\cos \theta') \quad (36)$$

$$G_{nm} = \frac{1}{j \omega \epsilon_0 R} \epsilon_m O_{nm} h_n^{(2)'}(\beta_0 R) j_n(\beta_0 r') P_n^m(\cos \theta') \quad (37)$$

where the primes denote a derivative with respect to the argument. Note that the functions $\Gamma_{nm}(\theta, \varphi)$, $\Lambda_{nm}(\theta, \varphi)$, $\Pi_{nm}(\theta, \varphi)$, $\Psi_{nm}(\theta, \varphi)$, $\Phi_{nm}(\theta, \varphi)$ and $\Theta_{nm}(\theta, \varphi)$ are dependent on the polar angle θ and the azimuthal angle φ for a fixed frequency or wave number β . To be able to solve the system of linear equations (28) and (29), the angular dependency must be eliminated. To this, first it requires expansion of the boundary condition equation (28) and (29) in PWSEs with separable variables, and matching each partial wave n , m . Accordingly, (28) and (29) is equated to the Laplace series as:

$$\begin{aligned} \sum_{n=0}^{\infty} \sum_{m=0}^n a_n \Gamma_{nm}(\theta, \varphi) + b_n \Lambda_{nm}(\theta, \varphi) - c_n \Pi_{nm}(\theta, \varphi) \\ = \sum_{n=0}^{\infty} \sum_{m=0}^n [\Delta_{nm} + b_n \Upsilon_{nm} - c_n \Omega_{nm}] Y_n^m(\theta, \varphi) \end{aligned} \quad (38)$$

$$\begin{aligned}
& \sum_{n=0}^{\infty} \sum_{m=0}^n a_n \Psi_{nm}(\theta, \varphi) + b_n \Phi_{nm}(\theta, \varphi) - c_n \Theta_{nm}(\theta, \varphi) \\
& = \sum_{n=0}^{\infty} \sum_{m=0}^n [W_{nm} + b_n U_{nm} - c_n V_{nm}] Y_n^m(\theta, \varphi)
\end{aligned} \tag{39}$$

Where $Y_n^m(\theta, \varphi)$ is spherical harmonic function. To remove the dependence on the polar angle and the azimuthal angle, the following orthogonality conditions can be applied to Equations (38) and (39):

$$\int_0^{2\pi} \int_0^{\pi} Y_n^m(\theta, \varphi) Y_p^q(\theta, \varphi) \sin \theta d\theta d\varphi = \delta_{np} \delta_{mq} \tag{40}$$

where $Y_p^q(\theta, \varphi)$ denotes the complex conjugate of the spherical harmonic function $Y_p^q(\theta, \varphi)$ and δ_{ij} is the Kronecker delta function. Equating the left- and right-hand sides in (38) and (39) for each partial wave and applying the orthogonality condition (40), a new system of linear equations is obtained which allows appropriate determination of the scattering coefficients b_n and c_n for the sphere. They are now rewritten as:

$$\begin{aligned}
& \sum_{p=0}^{\infty} \sum_{q=0}^p [\Delta_{(pq)} + b_n Y_{n(pq)} - c_n \Omega_{n(pq)}] = 0, \quad \sum_{p=0}^{\infty} \sum_{q=0}^p [W_{(pq)} + b_n U_{n(pq)} - c_n V_{n(pq)}] = 0 \\
& = 0
\end{aligned} \tag{41}$$

where

$$\Delta_{(pq)} = \sum_{n=0}^{\infty} \sum_{m=0}^n a_n \int_0^{2\pi} \int_0^{\pi} \Gamma_{nm}(\theta, \varphi) Y_p^q(\theta, \varphi) \sin \theta d\theta d\varphi \tag{42}$$

$$Y_{n(pq)} = \sum_{m=0}^n \int_0^{2\pi} \int_0^{\pi} \Pi_{nm}(\theta, \varphi) Y_p^q(\theta, \varphi) \sin \theta d\theta d\varphi \tag{43}$$

$$\Omega_{n(pq)} = \sum_{m=0}^n \int_0^{2\pi} \int_0^{\pi} \Lambda_{nm}(\theta, \varphi) Y_p^q(\theta, \varphi) \sin \theta d\theta d\varphi \tag{44}$$

$$W_{(pq)} = \sum_{n=0}^{\infty} \sum_{m=0}^n a_n \int_0^{2\pi} \int_0^{\pi} \Psi_{nm}(\theta, \varphi) Y_p^q(\theta, \varphi) \sin \theta d\theta d\varphi \tag{45}$$

$$U_{n(pq)} = \sum_{m=0}^n \int_0^{2\pi} \int_0^{\pi} \Phi_{nm}(\theta, \varphi) Y_p^q(\theta, \varphi) \sin \theta d\theta d\varphi \tag{46}$$

$$V_{n(pq)} = \sum_{m=0}^n \int_0^{2\pi} \int_0^{\pi} \Theta_{nm}(\theta, \varphi) Y_p^q(\theta, \varphi) \sin \theta d\theta d\varphi \tag{47}$$

The procedure for determining b_n and c_n requires first the determination of (42) through (47) by numerical integration. Once the scattering coefficients b_n and c_n are obtained, they can be used to compute the field components via inserting (21) through (23) into (24) through (27).

IV-Numerical Results and Discussions

We simulated the magnetic field for a point current dipole having a moment 700 nA.m, in a homogeneous sphere of radius 8 cm. As well as, the conductivity of the sphere is chosen 0.33S/m representative to the brain's white and gray matter were based on the available anatomical data [8-9].

A- Centered source

For the scenario of a centered current source, the coefficients b and c in (3) and (4) are calculated from (11). The magnetic field distribution in yz -plane due to a current dipole positioned at center of the sphere showed in figure 3 using a MATLAB[®] code. In this figure, for better coloring, the values are translated to dB.

Magnetic field distribution and pattern in both analyses are in good agreement and this shows that full-wave analysis can play a reliable role in future researches. As an important note that can be seen from figure 3, in quasi-static analysis the outside magnetic field is zero because in quasi-static regime a radial dipole creates no magnetic field outside the conductor [5]. In the application of magnetoencephalography (MEG), the full wave analysis shows attainable data in the out of the head in contrast with QSA method. In the other word, in full-wave analysis, the field is not zero and it shows that in MEG should not eliminated from the radial sources. It is worth to notice that in present traditional MEG analysis the radial oriented neurons doesn't detect at all while by using the full-wave analysis these neurons can be detected.

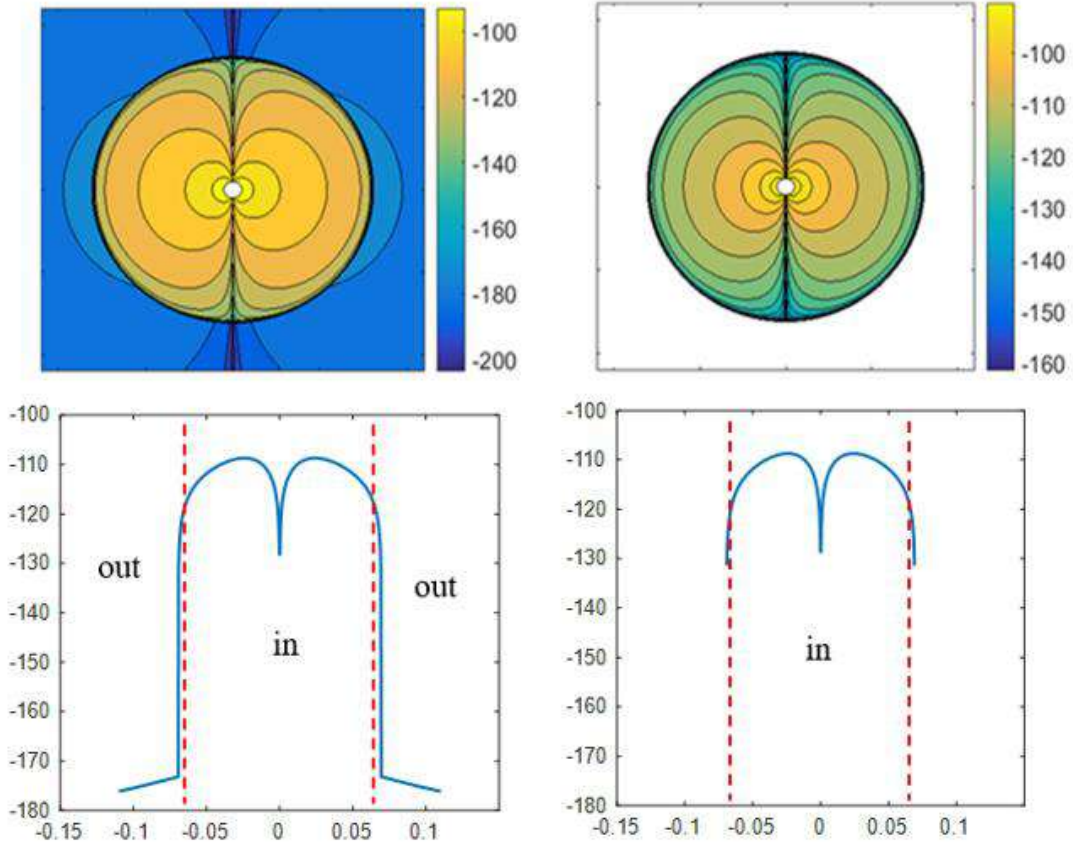


Fig. 3. The magnetic field pattern of a current dipole at center of a sphere: up-right: 2D simulation by using QSA; up-left: 2D simulation by using the full-wave analysis; down-right: sampled values of quasi-static magnetic field on horizontal line passed through center of sphere; down-left: sampled values of full-wave magnetic field on horizontal line passed through center of sphere.

For better comparison these two solutions, we use from the relative difference measure (RDM) [36].

$$RDM = \sqrt{\frac{\sum_{i=1}^N (B_i^F - B_i^Q)^2}{\sum_{i=1}^N (B_i^F)^2}} \quad (48)$$

In equation (48), i is the number of each node, B_i^Q is the magnetic field obtained from QSA and B_i^F is the magnetic field obtained from full-wave analysis. We divide the square of result in figure 3 into $N=700 \times 700$ node and sampled the magnetic field in each node. The full-wave magnetic field has saved in several frequency; from 1Hz to 1200Hz and RDM is calculated in each frequency. Figure 4 shows the RDM of magnetic field as a function of frequency in three values of conductivity. As can be seen in this figure, by increasing the frequency, the difference between QSA and full-wave results has been increased and the necessity of full-wave solution more sensed. Especially we see a difference between these two in the MEG frequency range (0.1-1000Hz). Furthermore, the higher the conductivity, the greater the difference and this indicates that the more conductive layers of the human head, lead to the greater the error in QSA.

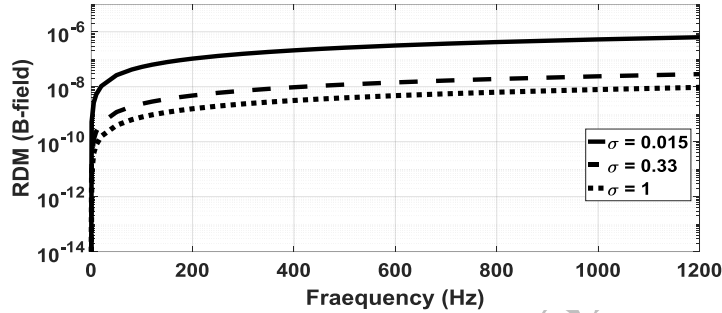


Fig. 4. RDM between quasi-static and full-wave magnetic field as a function of frequency for three values of conductivity

B- Off-center source

In the scenario of off-centre dipole, the coefficients b_n and c_n are calculated by developing a Mathematica code to obtain the numerical solution of the system of linear equations (41) through (47). Distributions of magnetic fields over the sphere's cross section at yz -plane produced by a z -directed dipole source positioned at $(r' = 2\text{cm}, \theta' = 60^\circ, \varphi' = 90^\circ)$ are shown in figure 5. The right picture is the magnetic field derived from QSA based on [7] and the left one is from full-wave analysis at 1000Hz based on the equations included in the section III-B. As can be seen, both simulations have same pattern and behaviour inside and outside of the sphere.

To better comparison between above two methods, the sampled values of fields on a horizontal line passed from center of sphere, i.e., on the line $z = 0$ in yz -plane, has been shown in figure 6. The right curve is the magnetic field derived from quasi-static approximation and the left one is from of full-wave analysis. As can be seen, the comparison two curves satisfies that the results obtained by PWSE full-wave are excellent. In the other off-center points, we have a challenge that described in the next section.

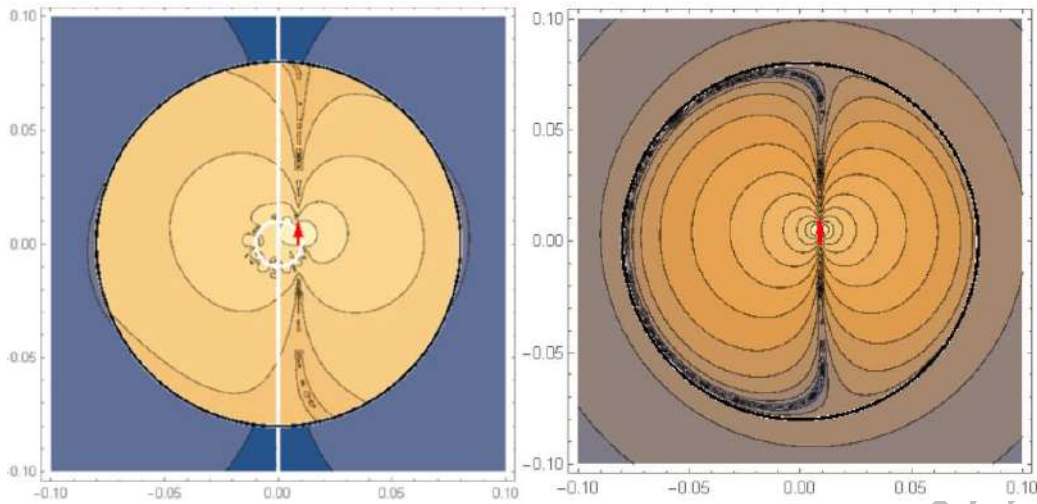


Fig. 5. The magnetic field pattern of a current dipole in a homogenous sphere with conductivity of 0.33S/m. right: quasi-static, left: full-wave

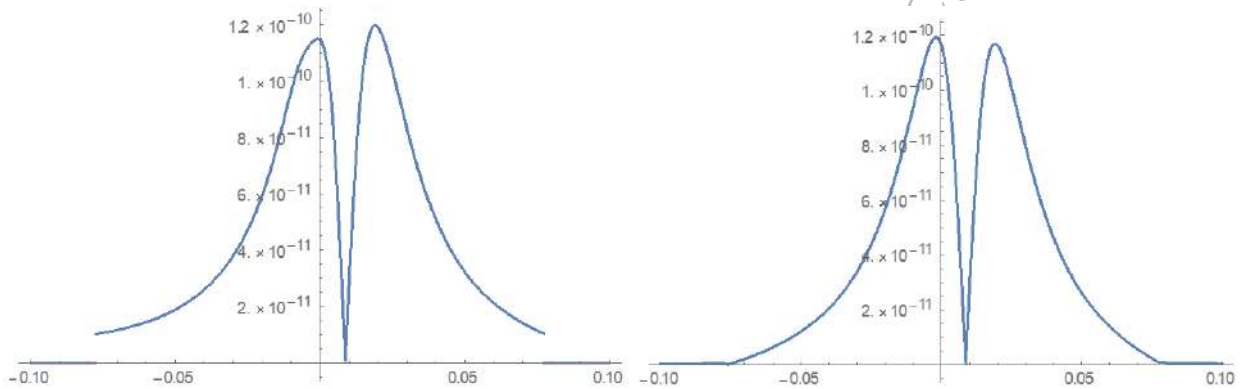


Fig. 6. The magnetic field in yz-plane sampled at line $z = 0$. left: full-wave, right: quasi-static

These results provide an advanced approach to accurately compute the electromagnetic fields of the brain for a relatively simple structure. This shows that for more complex structures (e.g. multilayer sphere and etc.) and near surface sources, the error rate of QSA results is significant. The accurate solving of full-wave analysis can help the peoples to interpret the EEG and MEG data more precisely and nearer to real in the inverse problem for source localization. Of course, it should be noted that the full-wave analysis requires more calculations in comparison with QSA, and this can be one of the drawback of this approach. But in future, this approach will be under more developments and its benefits become clearer, especially with powerful processing and modern measurement equipment.

V-Convergence of Addition Theorem

Addition theorem is a useful technique in mathematical solution of electromagnetic and acoustic scattering problems. It is, really, a series expansion of off-center Bessel and Hankel functions to distinct field point and source point from each other. In other words, the addition theorem transforms the implicit form of Bessel and Hankel functions into the explicit form that referred to the origin. The addition theorem of spherical Hankel function of zero-order and second kind is given in the following Equation:

$$h_0^{(2)}(|\vec{r} - \vec{r}'|) = \begin{cases} \sum_{n=0}^{\infty} (2n+1)h_n^{(2)}(r')j_n(r)P_n(\cos \xi), & r < r' \\ \sum_{n=0}^{\infty} (2n+1)h_n^{(2)}(r)j_n(r')P_n(\cos \xi), & r > r' \end{cases} \quad (49)$$

where $\cos \xi = \cos \theta \cos \theta' + \sin \theta \sin \theta' \cos(\varphi - \varphi')$ and $|\vec{r} - \vec{r}'| = \sqrt{r^2 + r'^2 - 2rr' \cos \xi}$.

In these equations ξ is angle between r and r' and $\vec{r} = (r, \theta, \varphi)$ and $\vec{r}' = (r', \theta', \varphi')$ are location of field point and source point respectively. In other words, this equation attributes an out of center source to the summation of weighted centered sources. This enables the engineers to solve many problems of acoustic and electromagnetic scattering. However, the addition theorem encounter to a critical problem in vicinity of r' , i.e. the lack of convergence in this region. To demonstrate this, we evaluate the addition theorem in $r = r'$. Thus, it should be concern to both sides of equation (49) by considering r equal to r' as derived in below:

$$h_0^{(2)}(\sqrt{r'^2 + r'^2 - 2r'r' \cos \xi}) = \sum_{n=0}^N (2n+1)h_n^{(2)}(r')j_n(r')P_n[\cos \xi] \quad (50)$$

In both side of equation (50), θ and φ (not r') are variables. For convenience we named the right-hand side of this equation as $f_R(\theta, \varphi)$ and the left-hand side as $f_L(\theta, \varphi)$. Then we draw the curve of each side of this equation, i. e., the curve of $f_R(\theta, \varphi)$ and $f_L(\theta, \varphi)$, in terms of θ and at a fix φ . In the right-hand side of equation (50), the number of terms (N) in summation is an important parameter. Increasing of this parameter reveals the convergence/divergence behavior of summation. The curve of real and imaginary parts of $f_R(\theta, \varphi)$ and $f_L(\theta, \varphi)$ is plotted in figure 7 for N=20.

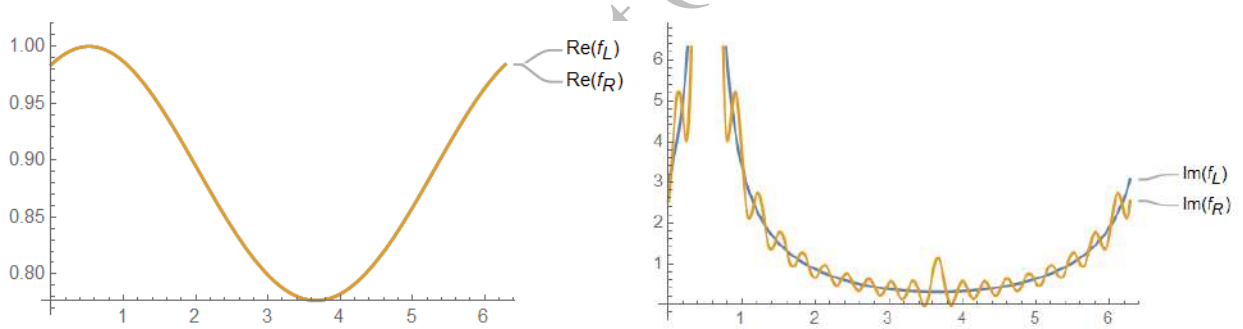


Fig. 7. Real and imaginary parts of $f_R(\theta, \varphi)$ and $f_L(\theta, \varphi)$

As can be seen in figure 7, the real part of two expression is exactly equal; this means that the series expansion of off-center spherical Hankel function is convergent. But the imaginary part of the series expansion of off-center spherical Hankel function $f_R(\theta, \varphi)$ has oscillations around its analytic formula. A question arises in this situation: what is the results while N is large? To answer this question, we have plotted the curves for larger value of N=50. Figure 8 shows the result. As can be seen, the imaginary part of series expansion is divergent and unstable at large N. The curve of imaginary part of both sides of equation (50) at $r = 0.9r'$ for N=50 is plotted in figure 9. This figure reveals the farther we go from the r' , the better the convergence situation. This indicates the improvement of series converges as moving away from r' . This challenge stops the extraction of other point results to compare QSA and Full wave PWSE. This is the subject of our future works.

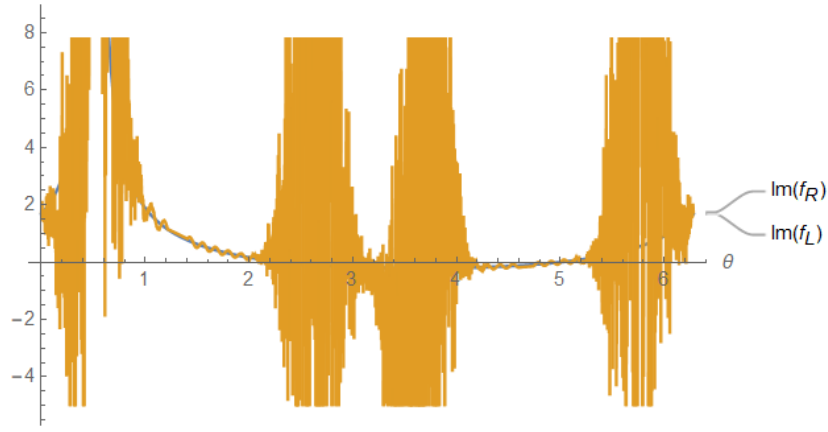


Fig. 8. Imaginary part of $f_R(\theta, \varphi)$ at $N=50$

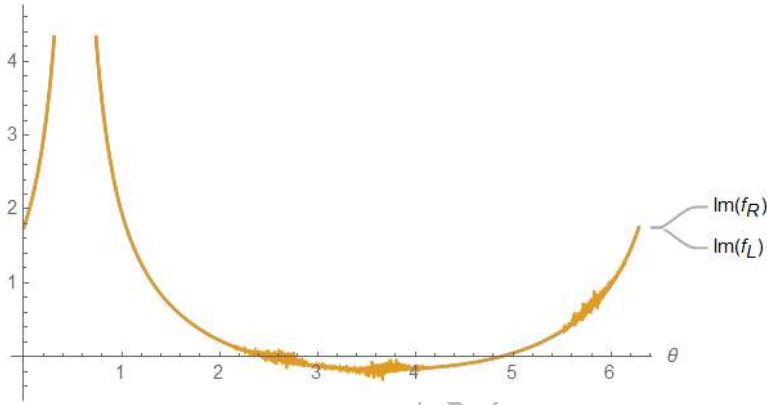


Fig. 9. Imaginary part of series expansion at $r = 0.9r'$ with $N=50$

VI-Conclusions

In this paper we have opened a new window to investigate of the brain waves by using method of full-wave instead of traditional quasi-static approximation (QSA). We have argued that why full-wave analysis for derivation of electric and magnetic fields of the brain is needed. We derived a full-wave solution for analytically predicting the electric and magnetic field from a current source (current dipole) positioned inside a spherical conductor. This is done by using a formal solution based on the auxiliary vector potential and scattering theory. The problem once solved for centered source and again for off-centered source. In the way of off-centered source, to apply appropriate boundary condition and eliminating angular dependence, the PSWE technique is used. The results showed the merits of full-wave solution over quasi-static solution and encouraged us to continue this way in professional format. The difference between these two in the MEG frequency range (0.1-100 Hz) shows the importance of the full-wave analysis for brain wave analysis. It should be noted that our detailed simulations will be presented in the next article, and our goal here was just representing the idea about full-wave analysis of brain waves.

References

- [1] Supek, S., & Aine, C. J. (2016). *Magnetoencephalography*. Springer-Verlag Berlin An.
- [2] Ito, T., Otsubo, H., Shiraishi, H., Yagyu, K., Takahashi, Y., Ueda, Y., ... & Saitoh, S. (2015). Advantageous information provided by magnetoencephalography for patients with neocortical epilepsy. *Brain and Development*, 37(2), 237-242.
- [3] Geselowitz, D. (1970). On the magnetic field generated outside an inhomogeneous volume conductor by internal current sources. *IEEE Transactions on Magnetics*, 6(2), 346-347.
- [4] Cuffin, B. N., & Cohen, D. (1977). Magnetic fields of a dipole in special volume conductor shapes. *IEEE Transactions on Biomedical Engineering*, (4), 372-381.
- [5] Sarvas, J. (1987). Basic mathematical and electromagnetic concepts of the biomagnetic inverse problem. *Physics in Medicine & Biology*, 32(1), 11.
- [6] De Munck, J. C., Van Dijk, B. W., & Spekreijse, H. E. N. K. (1988). Mathematical dipoles are adequate to describe realistic generators of human brain activity. *IEEE transactions on biomedical engineering*, 35(11), 960-966.
- [7] Heller, L., Ranken, D., & Best, E. (2004). The magnetic field inside special conducting geometries due to internal current. *IEEE transactions on biomedical engineering*, 51(8), 1310-1318.
- [8] Petrov, Y. (2012). Anisotropic spherical head model and its application to imaging electric activity of the brain. *Physical Review E*, 86(1), 011917.
- [9] J. O. Nieminen and M. Stenroos, "The magnetic field inside a layered anisotropic spherical conductor due to internal sources," *Journal of Applied Physics*, vol. 119, no. 2023901, pp. 1-12, 2016.
- [10] Huerta, M. A., & Gonzalez, G. (1983). The surface potentials produced by electric sources in stratified spherical and prolate spheroidal volume conductors. *International Journal of Electronics*, 54(5), 657-671.
- [11] De Munck, J. C. (1988). The potential distribution in a layered anisotropic spheroidal volume conductor. *Journal of applied Physics*, 64(2), 464-470.
- [12] Giapalaki, S. N., & Kariotou, F. (2006, January). The complete ellipsoidal shell-model in EEG imaging. In *Abstract and Applied Analysis* (Vol. 2006). Hindawi.
- [13] Malmivuo, J. (2012). Comparison of the properties of EEG and MEG in detecting the electric activity of the brain. *Brain topography*, 25(1), 1-19.
- [14] Bossetti, C. A., Birdno, M. J., & Grill, W. M. (2007). Analysis of the quasi-static approximation for calculating potentials generated by neural stimulation. *Journal of neural engineering*, 5(1), 44.
- [15] Gratiy, S. L., Halmes, G., Denman, D., Hawrylycz, M. J., Koch, C., Einevoll, G. T., & Anastassiou, C. A. (2017). From Maxwell's equations to the theory of current- source density analysis. *European Journal of Neuroscience*, 45(8), 1013-1023.
- [16] Bédard, C., & Destexhe, A. (2009). Macroscopic models of local field potentials and the apparent 1/f noise in brain activity. *Biophysical journal*, 96(7), 2589-2603.
- [17] Jain, S., Mitra, R., & Wiart, J. (2015). Full Wave Modeling of Brain Waves as Electromagnetic Waves. *Progress In Electromagnetics Research*, 151, 95-107.
- [18] Balanis, C. A. (2012). *Advanced engineering electromagnetics*. John Wiley & Sons.
- [19] Mitri, F. G. (2015). Axisymmetric scattering of an acoustical Bessel beam by a rigid fixed spheroid. *IEEE Transactions on Ultrasonics, Ferroelectrics, and Frequency Control*, 62(10), 1809-1818.
- [20] Koubeissi, M. Z. and Azar, N. J. (2017). *Epilepsy Board Review a Comprehensive Guide*. (pp. 301-307), Springer, New York, NY, 2017.
- [21] Zakharova, T. V., Karpov, P. I., & Bugaevskii, V. M. (2017). Localization of the activity source in the inverse problem of magnetoencephalography. *Computational Mathematics and Modeling*, 28(2), 148-157.
- [22] Hämmäläinen, M., Hari, R., Ilmoniemi, R. J., Knuutila, J., & Lounasmaa, O. V. (1993). Magnetoencephalography—theory, instrumentation, and applications to noninvasive studies of the working human brain. *Reviews of modern Physics*, 65(2), 413.
- [23] Geselowitz, D. B. (1967). On bioelectric potentials in an inhomogeneous volume conductor. *Biophysical journal*, 7(1), 1-11.
- [24] Zhang, Z. (1995). A fast method to compute surface potentials generated by dipoles within multilayer anisotropic spheres. *Physics in medicine & biology*, 40(3), 335.
- [25] Doschoris, M., & Kariotou, F. (2017). Mathematical foundation of electroencephalography. *Electroencephalography*.

- [26] Plonsey, R., & Heppner, D. B. (1967). Considerations of quasi-stationarity in electrophysiological systems. *The Bulletin of mathematical biophysics*, 29(4), 657-664.
- [27] Scheer, H. J., Fedele, T., Curio, G., & Burghoff, M. (2011). Extension of non-invasive EEG into the kHz range for evoked thalamocortical activity by means of very low noise amplifiers. *Physiological measurement*, 32(12), N73.
- [28] Fedele, T., Scheer, H. J., Burghoff, M., Curio, G., & Körber, R. (2015). Ultra-low-noise EEG/MEG systems enable bimodal non-invasive detection of spike-like human somatosensory evoked responses at 1 kHz. *Physiological measurement*, 36(2), 357.
- [29] Baranga, A. B. A. (2010, December). Brain's magnetic field: a narrow window to brain's activity. In *Electromagnetic field and the human body workshop*.
- [30] Dang, H. B., Maloof, A. C., & Romalis, M. V. (2010). Ultrahigh sensitivity magnetic field and magnetization measurements with an atomic magnetometer. *Applied Physics Letters*, 97(15), 151110.
- [31] Albanese, R., & Monk, P. B. (2006). The inverse source problem for Maxwell's equations. *Inverse problems*, 22(3), 1023.
- [32] Wilson, H. R. (1999). Spikes, decisions, and actions: the dynamical foundations of neurosciences.
- [33] Kuiken, T. A., Stoykov, N. S., Popovic, M., Lowery, M., & Taflove, A. (2001). Finite element modeling of electromagnetic signal propagation in a phantom arm. *IEEE Transactions on neural systems and rehabilitation engineering*, 9(4), 346-354.
- [34] Vorwerk, J., Cho, J. H., Rampp, S., Hamer, H., Knösche, T. R., & Wolters, C. H. (2014). A guideline for head volume conductor modeling in EEG and MEG. *NeuroImage*, 100, 590-607.
- [35] Harrington, R. F. (2001). *Time-harmonic electromagnetic fields*. IEEE press.
- [36] Meijs, J. W., Weier, O. W., Peters, M. J., & Van Oosterom, A. D. R. I. A. A. N. (1989). On the numerical accuracy of the boundary element method (EEG application). *IEEE transactions on biomedical engineering*, 36(10), 1038-1049.